Absolute sensitivity calibration of an extreme ultraviolet spectrometer for tokamak measurements

R Guirlet, Jl Schwob, O Meyer, S Vartanian

Absolute sensitivity calibration of an extreme ultraviolet spectrometer for tokamak measurements

R. Guirlet[a,1], JL. Schwob[b], O. Meyer[a], S. Vartanian[a]

[a]CEA, IRFM, F-13108 St-Paul-lez-Durance, France

[b]Racah Institute of Physics, Hebrew University of Jerusalem, Israel

Abstract

An extreme ultraviolet spectrometer installed on the Tore Supra tokamak has been calibrated in absolute units of brightness in the range 10-340 Å. This has been performed by means of a combination of techniques. The range 10-113 Å was absolutely calibrated by using an ultrasoft-X ray source emitting six spectral lines in this range. The calibration transfer to the range 113-182 Å was performed using the spectral line intensity branching ratio method. The range 182-340 Å was calibrated thanks to radiative-collisional modelling of spectral line intensity ratios. The maximum sensitivity of the spectrometer was found to lie around 100 Å. Around this wavelength, the sensitivity is fairly flat in a 80 Å wide interval. The spatial variations of sensitivity along the detector assembly were also measured. The observed trend is related to the quantum efficiency decrease as the angle of the incoming photon trajectories becomes more grazing.

Keywords: extreme ultraviolet; spectroscopy; tokamaks; absolute calibration

1. Introduction

Extreme ultraviolet (EUV) spectroscopy is used extensively in various plasma physics research fields such as astrophysics and inertial and magnetic fusion. Its main interest resides in the detailed information it provides on the various species present in a plasma. It thus helps determine the qualitative composition of a plasma by the observation and identification of the spectral lines emitted by the ion species of the plasma. The density of the various emitting ions can also be deduced from spectroscopic measurements provided certain experimental conditions are fulfilled. One of them is that the spectral line intensities must be measured in absolute units. This necessitates that the spectroscopic instrument be calibrated in sensitivity.

[1] Corresponding author. Tel.: +33-442-25-38-85.
E-mail address: remy.guirlet@cea.fr

A commonly used method is the so-called line intensity branching ratio method [1, 2]. It consists of selecting spectral line pairs emitted by the same ion from one given upper level to two different lower levels and comparing their measured intensity ratio with the theoretical one. For this purpose, usually the spectrometer to be calibrated includes a visible line of sight as close as possible to the EUV line of sight and connected to a visible spectrometer (for which an absolute calibration is relatively easy). One line of the pair is chosen in the visible range, and thus the sensitivity of the EUV spectrometer at the second line wavelength can be deduced. This method has been used already many years ago on the TA 2000 torus [3, 4] and is still in use nowadays, for example at JET for the SPRED VUV spectrometer in the range 130-360 Å [5]. Another way of calibrating an EUV spectrometer in absolute intensity units is to compare the spectrometer signals with those of an already absolutely calibrated instrument, as was done in [6] in the soft-X ray range.

In the present work, the Tore Supra tokamak is equipped with a high resolution, duo-multichannel grazing incidence spectrometer [7] of the Schwob-Fraenkel type. Two interferometrically aligned, ruled, concave gratings are mounted permanently on the spectrometer. For most of the applications and in particular for the present measurements, a 600 g/mm grating blazed at 1.5° is used. It covers the 10-340 Å wavelength range. The spectrometer is supported by a mobile structure which allows to spatially scan the lower half of the plasma at a frequency 0.5 Hz.

Detection on this spectrometer is performed by means of two double microchannel plate (MCP) detector assemblies in chevron configuration mounted on two carriages moved independently along the materialised Rowland circle. The range of one detector is limited on one end by the shortest wavelength mechanically accessible and on the other end by the second detector assembly. It is thus called the 'short wavelength' (or SW) detector. Conversely, the other assembly is limited by the SW detector and the longest wavelength mechanically accessible, hence its name: 'long wavelenth' (or LW) detector. The electrons produced in the microchannels by impact of the incident EUV photons are converted into visible photons by phosphor screens behind the MCPs and recorded by PDA (photodiode array) cameras (one for either MCP assembly). An example of a spectrum recorded on the LW detector is shown in Fig. 1.

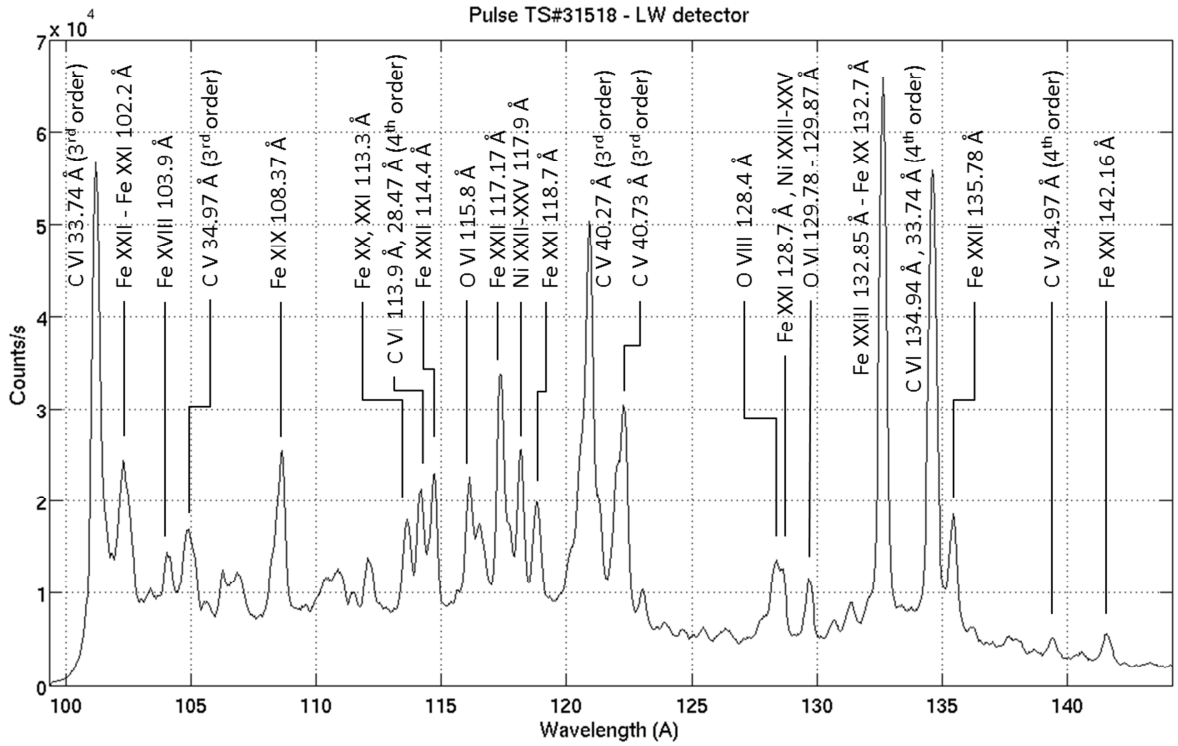

Figure 1: *Spectrum recorded by the long wavelength detector with identification of the most prominent lines.*

This spectrometer is not built with a visible line of sight so we could not use the branching ratio method exactly as presented in **[1]**. For the short wavelength part of the accessible domain we have used a combination of methods which are reported in this article. Section 2 describes the use of an ultrasoft-X ray source for absolute calibration in the 10-113 Å range. Section 3 describes the method used for calibration in the longer wavelength range, which combines the branching ratio method with a comparison of line intensity ratio measurements with collisional-radiative calculations, a method already used in **[8]**. Section 4 contains the results with a discussion on the uncertainties and a study of the spatial variation of the detector sensitivity. Section 5 presents a summary and conclusions.

2. Sensitivity calibration in the short wavelength range

2.1 Experimental setup and method

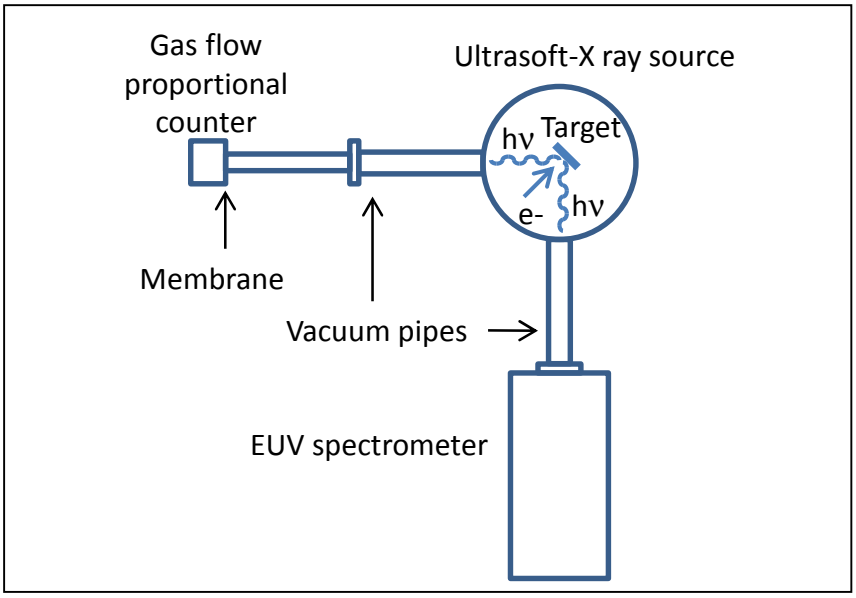

Figure 2: *Absolute calibration setup with the ultrasoft-X ray Manson source*

Target element	Wavelength (Å)
Mg	9.9
O	23.7
N	31.6
C	44.4
B	67.0
Be	113.0

Table 1: *List of emitting elements in the various targets and wavelengths of the corresponding spectral lines.*

In the short wavelength range, an absolute calibration was performed in the spectroscopy laboratory with the help of a Manson Model 5 multi-anode ultrasoft-X ray source **[9]**. The set-up is sketched on **Fig. 2**. The source emits photons at a given wavelength (the so-called Kα line) by electron beam impact on targets (playing the role of anodes for the electrons) of various materials. A carousel of six targets allows to produce as many spectral lines between 9.9 and 113 Å (see **Table 1**).

A gas flow proportional counter (GPC) is placed at 45° from the electron beam axis (a setup very similar to the one used in **[10]**) to monitor the photon emission which can be as high as 10^{12} photons/(s.sr). The GPC is set up so that it has a 100% efficiency. In order to preserve its operating pressure, which is different from that in the source volume, a membrane

is placed in front of the counter as a separation from the source volume. The membrane transmission factor T_{GPC} depends on the wavelength, as shown in **Table 2**.

Wavelength (Å)	9.9	23.7	31.6	44.4	67.0	113.0
T_{GPC} (%)	55	42	32	19	50	37

Table 2: *transmission factor of the membrane in front of the gas flow proportional counter*

In addition, we have used a grid filter (transmission $T_F = 0.108$) to attenuate the GPC signal. The photon rate (in s^{-1}) measured by the GPC is thus given by:

$$N^m_{GPC}(\lambda) = T_{GPC}(\lambda) \times T_F \times N^i_{GPC}(\lambda) \quad (1)$$

where $N^i_{GPC}(\lambda)$ and $N^m_{GPC}(\lambda)$ are the incident and measured photon rates respectively.

The spectrometer beam line is placed in a position symmetric to the GPC with respect to the electron beam to take advantage of the photon emission symmetry around the electron beam axis. The ratio of the photon rate incident on the spectrometer $N_{sp}^i(\lambda)$ to the photon rate $N^i_{GPC}(\lambda)$ incident on the GPC using a given target is equal to the solid angle ratio of the two detectors:

$$\frac{N^i_{sp}(\lambda)}{N^i_{GPC}(\lambda)} = \frac{\Omega_{sp}}{\Omega_{GPC}} \quad (2)$$

Note here that $N_{sp}^i(\lambda)$ represents the total number of photons within the whole spectral line width excluding the background in the same spectral interval.

The spectrometer sensitivity at wavelength λ is defined as the ratio of the measured count rate to the incident photon rate:

$$\eta(\lambda) = \frac{N^m_{sp}(\lambda)}{N^i_{sp}(\lambda)} \quad (3)$$

where $N_{sp}^m(\lambda)$ is the count rate measured by the spectrometer readout and acquisition system (expressed in counts/s in our setup). Due to the 100% efficiency of the gas counter and using **Eqs. 1** and **2**, one has:

$$N^i_{sp}(\lambda) = \frac{\Omega_{sp}}{\Omega_{GPC}} N^i_{GPC}(\lambda) = \frac{\Omega_{sp}}{\Omega_{GPC}} \frac{N^m_{GPC}(\lambda)}{T_{GPC}(\lambda) T_F}$$

and thus:

$$\eta(\lambda) = \frac{N_{sp}^{m}(\lambda)}{N_{GPC}^{m}(\lambda)/\left(T_{CP}(\lambda)T_F\right)} \frac{\Omega_{GPC}}{\Omega_{sp}} \quad (4)$$

The spectrometer sensitivity can thus be deduced from the geometric parameters of the setup, which are known, and the measurements of the detectors.

The tokamak plasma observed with the spectrometer is an extended light source. The measurement performed by the spectrometer is thus the radiance (also commonly called brightness) defined as:

$$B = (4\pi)^{-1} \times \int \varepsilon(l) dl \quad \text{[photons / (cm}^2 \text{ sr s)]} \quad (5)$$

where ε (in $cm^{-3}s^{-1}$), called emissivity, is the photon rate emitted by plasma unit volume in a given spectral line and *l* is the abscissa along the line of sight. The integral is performed over the whole line of sight path within the plasma. The quantity we aim at determining is the brightness calibration coefficient *K(λ)* defined by:

$$B(\lambda) = K(\lambda) \times N_{sp}^{m}(\lambda) \quad (6)$$

over the whole wavelength range of the spectrometer. This quantity is crucial for plasma applications since it is needed to relate the measured quantity $N_{sp}^{m}(\lambda)$ with the density of the emitting ions. It can be obtained in the following manner. When a spectral line emitted in the plasma is observed, the incident photon rate is by definition of η(λ):

$$N_{sp}^{i}(\lambda) = \frac{N_{sp}^{m}(\lambda)}{\eta(\lambda)} \quad (7)$$

The spectral line brightness is thus given by:

$$B(\lambda) = \frac{N_{sp}^{i}(\lambda)}{(S\Omega)_{sp}} = \frac{N_{sp}^{m}(\lambda)}{\eta(\lambda) \times (S\Omega)_{sp}} \quad (8)$$

where $(S\Omega)_{sp}$ is the spectrometer geometric etendue (here *S* is the entrance slit area). The brightness calibration coefficient is thus given by:

$$K(\lambda) = \frac{1}{\eta(\lambda) \times (S\Omega)_{sp}} \quad (9)$$

and is expressed in [photons/(s cm^2 sr)]/(counts/s).

2.2 Results and comparison with a previous calibration

The method exposed in the previous section has been applied to both the 'shorter wavelength' (SW) and 'longer wavelength' (LW) detectors. The brightness calibration coefficient has been determined for the six wavelengths available with the calibration source. It is shown in **Fig. 3**. As the LW detector cannot be positioned to observe wavelengths shorter than 77 Å, only the coefficient at 113 Å could be obtained by this method. Interestingly, it has almost the same value as for the SW detector at the same wavelength. This observation results from the fact that the two detectors are practically identical. It also denotes the accuracy of the interferometric alignment of the spectrometer **[7]** and of the mechanical positioning of the detectors along the Rowland circle to better than 25 µm. In the following we will thus not distinguish between the two detectors on the calibration curves.

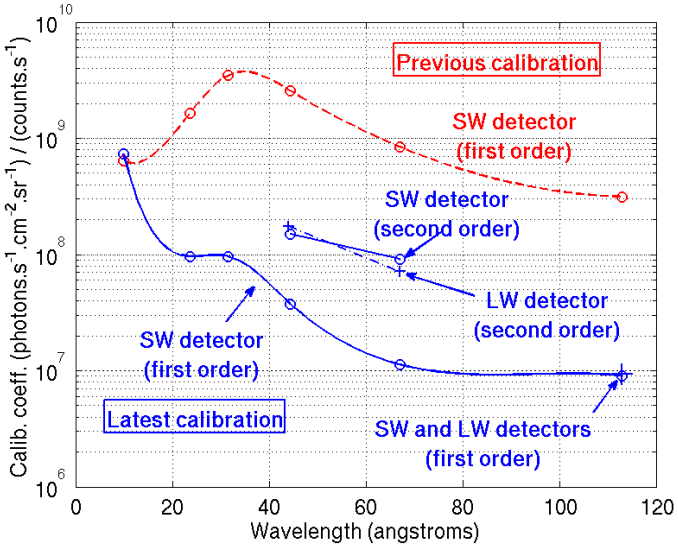

Figure 3: *Absolute brightness calibration coefficient as a function of wavelength. SW detector: (red ○ and dashed line) previous calibration in the first order and (blue ○ and solid line) latest calibration in the first and second orders. LW detector: (blue + and dashed-dotted line) latest calibration in the first two orders.*

It can be seen from the slope of the calibration curve that on the short wavelength side the spectrometer sensitivity (proportional to $1/K$) decreases with decreasing wavelength, which illustrates the difficulty to measure spectral line intensities below 10 Å with this 600g/mm gold coated ruled grating. The comparison of the latest calibration curve with the previous one shows that the various improvements to the spectrometer (use of two microchannel plates in chevron configuration for each detector assembly, installation of a new grating, better performance PDA camera) have enhanced the spectrometer sensitivity by about a factor 30 over the whole calibrated wavelength range except below about 20 Å. The latter feature is most likely due to the characteristics of the previous 600 l/mm holographic grating which was platinum coated, while the new grating is a ruled one and gold coated with a steeply decreasing efficiency toward the very short wavelengths below 15 Å.

As this new grating is not designed to suppress the higher diffraction orders, the ultrasoft X- ray source lines at 44.4 Å and 67 Å have also been observed in the second order and have been used for the calibration, as shown in **Fig. 3**. They show that the spectrometer sensitivity in the second order is poorer than in the first order, but only by a factor of 5 to 8. We have actually observed intense spectral lines emitted by the tokamak plasma in as high an order as the 7^{th} or the 8^{th}. Notice that the second order calibration is almost the same for the SW and the LW detectors, another indication that the two detectors are practically identical.

3. Sensitivity calibration in the long wavelength range

3.1 Use of the branching ratio method

The mechanical design of the spectrometer presently equipped with two detector carriages sets a lower limit of about 77 Å to the spectral range accessible to the LW detector (this limit is actually reached when the SW detector carriage is itself positioned at the shortest possible wavelength position). The only line emitted by the ultrasoft X-ray calibration source above this limit, and thus the only available one for the LW detector calibration in the first order, is at 113 Å. Therefore, another method has to be used in order to calibrate the spectrometer up to its maximum wavelength, which reaches 340 Å with the routinely used 600 g/mm grating.

The first additional method we use here is the so-called branching ratio method **[1, 2]**, which we will now describe briefly. The emissivity ratio of two spectral lines of a given ion emitted by transitions from the same upper level to two different lower levels depends only on atomic constants and not on the plasma conditions. In tokamak plasmas the emission is completely dominated by spontaneous decay (rather than collisional de-excitation) so that the ratio can be written as:

$$\frac{\varepsilon_{ij}}{\varepsilon_{ik}} = \frac{n_i A_{ij}}{n_i A_{ik}} = \frac{A_{ij}}{A_{ik}} \tag{10}$$

where n_i is the population density of the upper level i and A_{ij} and A_{ik} are the Einstein coefficients for spontaneous decay from levels i to levels j and k respectively. This relation holds as long as neither spectral line is self-absorbed by the plasma, i.e. when the plasma optical thickness can be neglected, which is the case here since the impurity ion density is always far below the main plasma ion density of about 5×10^{19} m^{-3}. The effect of radiation trapping on the line brightness has been calculated using a mean transmission factor approach **[2, 11]** and the predictions were confirmed by measurements on the TA2000 torus **[4]**. It was found that for an optical thickness of the plasma below 0.1, the self-absorption is less than 3.5%. It is thus negligble in the present experimental conditions.

Using Eq. (5) it is easy to show that the same relation can be used for the brightness ratio B_{ij}/B_{ik} measured by a spectrometer along a line of sight through the plasma. The relation between the measured signal ratio and the brightness ratio can be deduced from **Eqs. 6** and **10**:

$$\frac{K(\lambda_{ij})N_{ij}^m}{K(\lambda_{ik})N_{ik}^m} = \frac{B_{ij}}{B_{ik}} = \frac{A_{ij}}{A_{ik}} \tag{11}$$

This leads to the relation:

$$\frac{K(\lambda_{ij})}{K(\lambda_{ik})} = \frac{N_{ik}^m}{N_{ij}^m}\frac{A_{ij}}{A_{ik}} \tag{12}$$

This relation shows that the ratio of calibration coefficients at two different wavelengths can be deduced from line intensity measurements, which can be performed using

the tokamak plasma itself as a calibration source, and from Einstein coefficients, which are well known atomic constants in our case. This relation can thus be used for *relative* calibration for the two wavelengths λ_{ij} and λ_{ik}. This is particularly useful to determine the absolute calibration factor at either wavelength when it is already known at the other. As already said, the latter application is often used for VUV spectrometers using a visible spectrometer having the same line of sight **[3,4,5]**.

As we did not have such a setup, we took advantage of the absolute calibration over the SW range described in the previous paragraph to calibrate the longer wavelength range by using spectral line pairs with one line below 113 Å (measured in absolute units with the SW detector) and the other at a wavelength to be calibrated above this value (measured with the LW detector). This procedure relies on the assumption that the two detectors have the same sensitivity at any given wavelength, an assumption supported by their identical design and by the identical absolute calibration coefficient found at 113 Å in Section 2.

In our case, the plasma emits few pairs of lines obeying the constraints imposed by the branching ratio method and the spectrometer wavelength coverage (two lines emitted from the same initial level of the same ion with a sufficient intensity, the wavelength of one between 10 and 113 Å, the other between 113 and 340 Å). Only two suitable pairs were found, emitted by Carbon, the dominant impurity in Tore Supra plasmas. They are shown in **Table 3**. The calibration coefficients at 28.5 Å and 27.0 Å are calculated by a linear interpolation between the two closest calibration points obtained in Section 2, namely 23.7 Å and 31.6 Å.

LW spectral line			SW spectral line			Theoretical intensity ratio A_{ij}/A_{ik}
Transition	λ (Å)	A_{ij} (s^{-1})	Transition	λ (Å)	A_{ik} (s^{-1})	
n=3 → n=2 (C VI)	182.2	5.72×10^{10}	n=3 → n=1 (C VI Lyβ)	28.5	7.23×10^{10}	0.79
n=4 → n=2 (C VI)	134.9	1.09×10^{10}	n=4 → n=1 (C VI Lyγ)	27.0	1.66×10^{10}	0.66

Table 3: *Pairs of spectral lines and theoretical intensity ratios which have been used for relative calibration of the spectrometer above 113* Å.

This method provides invaluable information in that it allows to link the absolute calibration in the shorter wavelength range with the relative calibration in the longer

wavelength range. Nevertheless it is clearly not sufficient to calibrate the whole longer wavelength range of the spectrometer coverage. A complementary method is presented below.

3.2 Collisional-radiative modelling of line intensity ratios

The results of the branching ratio method exposed in the previous paragraph do not depend on the experimental conditions such as the plasma parameters and their time evolution or the spectrometer line of sight geometry. However, as it has just been shown, there are in general very few pairs of spectral lines which can be used in a given experimental situation. Relaxing the constraint of an identical upper level for the spectral line pairs used for the calibration, we find many groups of lines emitted by a given ion in the plasma within the relevant wavelength range. The drawback is that the relative intensities of the lines within a group depend not only on atomic physics but also on the plasma parameters. They can be calculated in the frame of a collisional-radiative model (CRM).

This calibration method, less accurate than the branching ratio method, has been applied on the SPRED VUV spectrometer at JET for the 360-980 Å range using spectral lines from mostly low ionisation stages **[5]**. In the present work, we aimed at calibrating a shorter wavelength range (130-340 Å) than at JET. We also wanted to avoid using spectral lines emitted near the plasma edge, where the plasma parameters are not so well known (in particular the electron temperature). For both these reasons we did not select very low ionisation stages, as can be seen on **Table 4**.

Emitter	**Wavelength (Å)**	**Transition**
C IV	222.8	$1s^2 2s\ ^2S$ - $1s^2 5p\ ^2P^o$
	244.9	$1s^2 2s\ ^2S$ - $1s^2 4p\ ^2P^o$
	259.5	$1s^2 2p\ ^2P^o$ - $1s^2 5d\ ^2D$
	262.6	$1s^2 2p\ ^2P^o$ - $1s^2 5s\ ^2S$
	289.2	$1s^2 2p\ ^2P^o$ - $1s^2 4d\ ^2D$
	296.9	$1s^2 2p\ ^2P^o$ - $1s^2 4s\ ^2S$
	312.4	$1s^2 2s\ ^2S$ - $1s^2 3p\ ^2P^o$
C VI	**27.0**	**1 – 4 (Ly γ)**
	28.5	**1 – 3 (Ly β)**

	134.9 + 135.0	**2 – 4 (Balmer β)**
	182.1 + 182.2	**2 – 3 (Balmer α)**
O V	151.5	$2s2p\ ^3P^o$ - $2s4d\ ^3D$
	192.8 + 192.9	$2s2p\ ^3P^o$ - $2s3d\ ^3D$
O VI	129.8 + 129.9	$1s^2 2p\ ^2P^o$ - $1s^2 4d\ ^2D$
	150.1	$1s^2 2s\ ^2S$ - $1s^2 3p\ ^2P^o$
	172.9 + 173.1	$1s^2 2p\ ^2P^o$ - $1s^2 3d\ ^2D$
	183.9 + 184.1	$1s^2 2p\ ^2P^o$ - $1s^2 3s\ ^2S$
Fe XXIV	192.0	$1s^2 2s\ ^2S$ - $1s^2 2p\ ^2P^o_{3/2}$
	255.1	$1s^2 2s\ ^2S$ - $1s^2 2p\ ^2P^o_{1/2}$

Table 4: *Spectral lines used in the branching ratio method for absolute calibration transfer (in bold) and in the CRM line ratio method for relative calibration.*

In the collisional-radiative modelling, instead of expressing the line emissivity as a function of the population density of the initial level of the transition (as in **Eq. 10**), we use the total density n_z of the emitting ion. The emissivity of a given line between levels *i* and *j* can be written as:

$$\varepsilon_{ij} = n_e n_z PEC_{ij}(n_e, T_e), \tag{13}$$

where n_e and T_e are the electron density and temperature respectively. The PEC_{ij} quantity, called photon emission coefficient, is calculated with a collisional-radiative model (CRM). It depends in a complex way on the collisional and radiative atomic processes in the plasma, namely transitions between excited levels of the emitting ions, recombination onto and ionisation from excited levels. The PEC dependence on n_e is generally weak and will be neglected here. In the present case the PEC values were obtained from the ADAS data and model **[12]**.

From **Eq. 13** it can be deduced that the emissivity ratio of two lines *ij* and *kl* emitted by the same ion is equal to the PEC ratio. For the brightness, which is the quantity actually measured by the spectrometer, the situation is slightly more complex:

$$\frac{B_{ij}}{B_{kl}} = \frac{\int n_e n_z PEC_{ij}(T_e) dl}{\int n_e n_z PEC_{kl}(T_e) dl} \tag{14}$$

where the integration is done along the line of sight. The exact calculation requires that we know the spatial distribution of all quantities in the integrals, in particular the emitting ion density profile along the line of sight. The most accurate way to obtain this is from a dedicated transport study **[13]**, a sophisticated and somewhat lengthy procedure. Instead, we make here the rougher assumption that the PECs do not depend on T_e. This is verified in our case because the emitting layer of the selected ions in this study is very narrow. As an additional precaution, we have rejected lines with PECs depending strongly on the temperature in the T_e range where the emitting ion is abundant (e.g. C V 40.3 Å, $1s^2\ ^1S_0$ - $1s2p\ ^1P_1{}^o$). As a consequence, denoting T_e^{em} the electron temperature of the emitting layer, the measured brightness ratio will thus be approximately equal to the PEC ratio:

$$\frac{B_{ij}}{B_{kl}} = \frac{PEC_{ij}(T_e^{em})}{PEC_{kl}(T_e^{em})} \tag{15}$$

An accurate determination of T_e^{em} would require either a full transport study, as already mentioned, or enough lines of sight to determine experimentally the position of the emission layer. The weak T_e dependence requested from the PECs retained in this study allowed to estimate T_e^{em} witout loss of accuracy from the position of the emitting layers as calculated by a local ionisation balance calculation.

Denoting again N_{ij}^m the measured signal and $K(\lambda_{ij})$ the corresponding calibration coefficient, one gets by definition of the calibration coefficient (**Eq. 6**):

$$\frac{B_{ij}}{B_{kl}} = \frac{K(\lambda_{ij})}{K(\lambda_{kl})} \frac{N_{ij}^m}{N_{kl}^m} \tag{16}$$

Provided the calibration coefficient is known at one wavelength, say λ_{ij}, the coefficient at the other wavelength λ_{kl} can be obtained by using **Eq. 15**:

$$K(\lambda_{kl}) = K(\lambda_{ij}) \frac{N_{ij}^{m}}{N_{kl}^{m}} \frac{PEC_{kl}}{PEC_{ij}} \quad (17)$$

Comparing the calculated and measured C VI line brightness ratios, we have calculated the absolute calibration coefficients at 134.9 Å and 182.2 Å. Note that at 134.9 Å the Balmer β line is blended with the fourth order of the C VI Ly α line at 33.7 Å. In order to subtract the latter contribution it was necessary to estimate the grating efficiency in the fourth order. This was done by measuring the intensity of the well resolved C V 34.97 Å line in the first and fourth orders in identical pulses designed for the calibration described here (see next Section). This allowed us to deduce that the grating efficiency in the fourth order with respect to that in the first order is about 10% at this wavelength. The contribution of the fourth order C VI Ly α line to the measured 134.9 Å intensity was then calculated using the measured first order C VI Ly α line intensity and the fourth order efficiency. It was then subtracted from the measured intensity at 134.9 Å before the calibration coefficients were calculated.

Then we interpolate the calibration coefficient of the 150.1 Å line of the O VI group between the values at 134.9 Å and 182.2 Å. From there, we use **Eq. 17** with the O VI line group to obtain the calibration coefficients at 129.9 Å, 173 Å and 184 Å. Then with the same hypothesis we obtain the 151.5 Å (O V group) calibration coefficient, and this allows us to obtain the calibration coefficient at the second wavelength of the O V group, 192.9 Å. With the same reasoning, we obtain the calibration coefficients at 192.0 Å and 255.1 Å (Fe XXIV group) and at the six wavelengths of the C IV group. It has been checked that the final result (the curve which will be fitted to the data points) remains within the error bars if the order in which the line groups are added is changed.

4. Results and uncertainties

4.1. Results

A series of identical, ohmic pulses have been performed to record the useful spectral line brightnesses (Tore Supra pulses TS#31512 to TS#31519). The plasmas are found to be

very stationary and reproducible so there was no need to perform a multi-pulse statistical study of the line ratios. The spectrometer was used in its spatial scanning mode, which means that the whole spectrometer was rotated around a horizontal axis located in front of the apparatus. In this mode of operation, the lower half of the plasma (see **Fig. 4**) could be scanned at a period of 0.5 Hz.

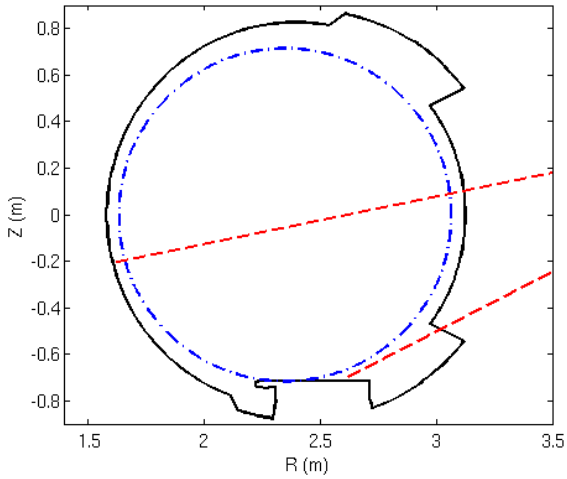

Figure 4: *Poloidal cross section (solid line) of the tokamak vessel, (dashed-dotted line) of the plasma last closed flux surface and (dashed line) of the extreme positions of the line of sight.*

Both the spectral line shapes and the radial profiles were used to reject blended lines. In the case of the Fe XXIV lines, observed to be blended in **[5]**, the analysis of the radial brightness profiles allows to distinguish them from blended light species lines.

The calibration coefficients obtained with this method have been added to the results obtained in Section 2.2. The overall calibration curve is shown in **Fig. 5**. It shows a broad minimum (corresponding to a maximum in sensitivity) around 100 Å over a range of about 70 Å. The spectrometer sensitivity decreases steeply on both sides, although in the long wavelength direction the slope tends to become lower. This indicates that with the same grating a modified spectrometer with a longer mechanical range for the detector would be sensitive enough to provide information over a broader wavelength range. This has been done for the Schwob-Fraenkel spectrometer installed on the Berlin EBIT experiment **[14, 15]**. On the contrary, in the short wavelength direction the slope is steeper and steeper. This indicates that extending the mechanical range to shorter wavelengths would not provide additional useful information below 10 Å.

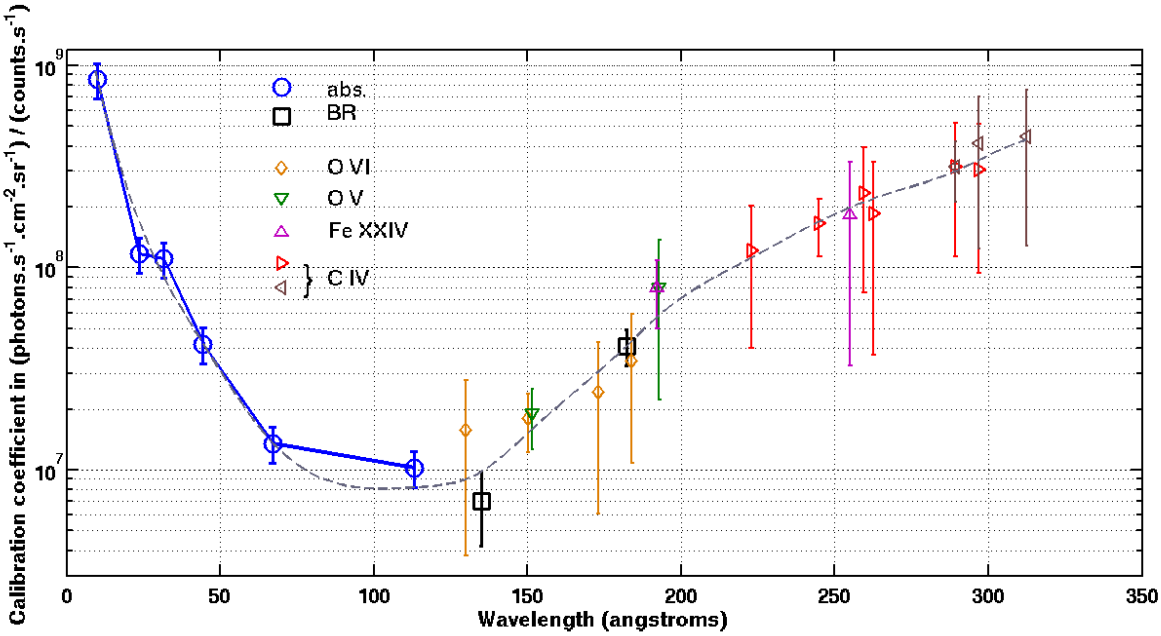

Figure 5: *Absolute brightness calibration in lab (solid line with ○), calibration transfer using the branching ratio method (□) and relative calibration using the CRM of line ratios with plasma (the symbols are explained on the figure). The grey dashed line is a spline among the points and is adopted as the final calibration curve.*

4.2. Uncertainties

In the wavelength range absolutely calibrated with the ultrasoft-X ray source (9.9 - 113 Å), the main uncertainty is that associated with the spectral line intensities measured with the spectrometer. It is mostly due to the uncertainty on the background estimate, which can be difficult for the weaker lines of the calibration source. The uncertainty on these intensities is at maximum 10% (it can be as low as 5% for the stronger lines). In addition, we estimate an uncertainty of 10% to take account of the geometric aperture uncertainty. The uncertainty on the proportional gas counter measurements is negligible compared to those associated with the spectrometer measurements. We have thus a global uncertainty of 20% for the calibration coefficients up to 113 Å.

For the calibration points using the branching ratio method, we must take into account the time fluctuations of the two spectral line intensities used for each point. These fluctuations are not negligible even during the stationary phase of the plasma. They are actually much larger than the statistical error (which is the square root of the time average signal if a Poisson distribution is assumed). The total uncertainty is thus estimated to 40% at 134.9 Å and 32% at 182.2 Å.

For the CRM calibration method, a part of the uncertainty associated with the reference line (at wavelength λ_0) of a given line group is determined from the time fluctuation of the measured signal as discussed in the previous paragraph. To this fluctuation uncertainty, an uncertainty of 30% is added, corresponding to the interpolation of this reference line between two already calibrated wavelengths. For any other line (wavelength λ) of the group, the uncertainty is deduced from **Eq. 17**:

$$\frac{\Delta K(\lambda)}{K(\lambda)} = \frac{\Delta K(\lambda_0)}{K(\lambda_0)} + \frac{\Delta\left(\frac{PEC(\lambda)}{PEC(\lambda_0)}\right)}{\frac{PEC(\lambda)}{PEC(\lambda_0)}} + \frac{\Delta N^m(\lambda)}{N^m(\lambda)} + \frac{\Delta N^m(\lambda_0)}{N^m(\lambda_0)} \qquad (18)$$

The relative uncertainties on the signals $N^m(\lambda)$ and $N^m(\lambda_0)$ are calculated from the time fluctuations of the measurements, as said above. The uncertainty on the PECs themselves is difficult to assess and not always available in the literature. It seems that a global value of 30% for all PEC ratios reflects satisfactorily both the accuracy of the atomic physics calculations and the residual PEC ratio dependence on T_e^{em} (see above the discussion about **Eq. 15**) .

For a practical purpose, a curve has been fitted on the points in **Fig. 5**. The most satisfactory result was obtained with a spline. Below 120 Å the 20% uncertainty estimated for the absolute calibration points can be retained. Between 120 and 180 Å, where line intensity branching ratios were available, an uncertainty of about 35% is estimated. Above this wavelength, a value of 50% reflects satisfactorily the spreading and uncertainties of the relative calibration points. In this range, the uncertainty might be an underestimate of the actual uncertainty due to the use of the CRM, for which the uncertainties are not well known.

5. Spatial variations of the detector response

The tolerances of the spectrometer design and realisation are very tight, so that most mechanical pieces are positioned to less than 25 µm. Nevertheless, the response of the detector assembly along its length (i. e. along the wavelength direction) is not perfectly

uniform. It can be due to several reasons such as the small inhomogeneities of the multichannel plate and phosphor screen responses, the transmission of the fiber optics bundle or the quantum efficiency dependence on the photon incidence angle on the MCP input face.

As the non-uniformity and the spatial variation of the detector response play a role in the estimate of the spectral line absolute brigthnesses, it has been measured for the LW assembly. The simplest way of doing this measurement is to select a spectral range containing well isolated spectral lines and perform several measurements, moving the detector by small position shifts between measurements in such a way that the spectral lines would strike different parts of the MCP.

Due to programme constraints, this method could not be applied in the spectroscopy laboratory. Therefore we have used the same series of identical discharges on the Tore Supra tokamak as for the calibration. During this series, the detectors were moved in a limited number of positions. As a result of this procedure, many spectral lines could be measured at a few positions on the detector. By comparing the spectrometer measurements of a given spectral line in the various positions and synthetising the results for all lines, we were able to deduce the non-uniformity and spatial variation of the detector assembly response. The list of the lines used for this procedure is given in **Table 5**.

Wavelength (Å)	Emitter
129.9	O VI
132.9	Fe XXIII
134.9	C VI 2-4 (+ Ly α 4^{th} order)
135.8	Fe XXII
238.5	O IV, C IV
241.5	C V (40.3 Å 6^{th} order)
244.9	C IV
281.9	C V
284.1	Fe XV
289.2	C IV
292.0, 291.3	Ni XVIII, C III

Table 5: *List of spectral lines and corresponding emitters for the evaluation of the non-uniformity and spatial variation of the detector response.*

The synthesis of all these measurements is presented on **Fig. 6**. The results show that the intensity response is a decreasing function of the spectral line position in the direction of increasing pixel number (corresponding to increasing wavelengths) on the MCP detector in the useful range (between pixels 70 and 900 for the LW detector). The measurements show that the response at both ends of the detector (below pixel 70 and above pixel 900) is substantially degraded with respect to the major part of the detector range. This is due to the fact that the size of the PDA is slightly larger than the fiber optics bundle size. One notices that the unuseful portion on the large pixel number extremity is wider than that on the small pixel number extremity. This indicates that the bundle is not perfectly centred on the photodiode array. Both ends of the detector have thus been excluded from the study.

A straight line has been fitted to the data and the correction factor curve thus obtained has been normalised so that it is 1 in the middle of the detector (pixel 512 here). The spreading of the points around a given position and wavelength in **Fig. 6** indicates that the measurement fluctuations are dominant over the spatial inhomogeneities along the detector. The response decrease along the detector seems to be mostly related to the varying response of the MCP with the photon incidence angle. Indeed it is known that the MCP quantum efficiency decreases as the incoming photon angle with the grating plane becomes more grazing.

In **Fig. 6**, the average slope for the group of lines around 130 Å does not show a significant difference with that for the group in the range 240-292 Å (it would correspond to a response difference of less than 3%). Therefore we can consider that the wavelength dependence of the detector response spatial variation can be neglected. As no data in the short (10-70 Å) wavelength range are available for this calibration campaign, the average decrease of **Fig. 6** was used to correct all the line intensity measurements performed for the Manson source and the branching ratio methods (**Figure 5** includes these corrections.) As the intensity response curve introduces a maximum correction of about 20%, which is small compared with the global uncertainty estimated in Section 4.2, it was not necessary to make this correction for the CRM calibration above 200 Å.

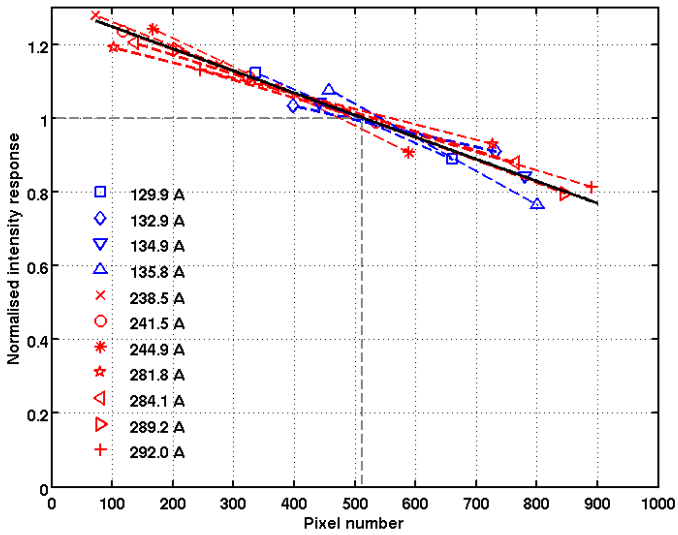

Figure 6: *Intensity response of the LW detector assembly as a function of the line position on the detector (measured in pixels). Each symbol represents a different spectral line (see list on Table 4). Dashed line: final correction factor.*

6. Summary and conclusion

The grazing incidence spectrometer operated on Tore Supra with a 600g/mm grating blazed at 1.5° has been absolutely calibrated over most of its wavelength coverage, i. e. 9.9-312 Å. For the lower part of this domain (9.9-113 Å) we have used an ultrasoft-X ray source calibrated against a gas flow proportional counter set up with a 100% efficiency. For the rest of the wavelength domain we have used the branching ratio method for absolute calibration transfer and collisional-radiative modelling of line intensity ratios for relative calibration.

The results show that the spectrometer sensitivity has improved with respect to the previous setup thanks to the new grating and the double multichannel plates in chevron configuration. The spectrometer is most sensitive in the 50-200 Å range, with a steep decrease below 50 Å. On the long wavelength side the sensitivity decrease is not as steep. In fact, after the present calibration procedure we have exchanged the 600 g/mm grating with a 300 g/mm one and obtained useful measurements up to 680 Å.

The uncertainties have been calculated for each individual calibration wavelength. Due to the variety of methods used for the whole wavelength range, it is not straightforward to determine a precise global uncertainty. We estimate a 20% uncertainty below 120 Å, where direct absolute calibration was obtained with the ultrasoft-X ray source, and 35% in the range 120-180 Å where the line branching ratio method was used. In the range above 180 Å where only the relative calibration procedure (collisional-radiative modelling of line intensity ratios)

was available, the uncertainty is estimated to 50% or even more. This reflects the larger uncertainties and the spreading of the individual calibration points in the LW range.

Bibliography

[1] E. Hinnov and W. Hofmann, J. Opt. Soc. Am. 53 (1963) 1259

[2] J.L. Schwob and C. Breton, C. R. Acad. Sc. 261 (1965) 1476

[3] J.L. Schwob, C. R. Acad. Sc. 262 (1966) 1264

[4] J.L. Schwob, CEA report R-3359 (1969)

[5] K. Lawson, I. Coffey, J. Zacks, M.F. Stamp and JET-EFDA contributors, J. Instr. 4 (2009) P04013

[6] J. Park, G.V. Brown, M.B. Schneider, H.A. Baldis, K.V. Cone, R.L. Kelley, C.A. Kilbourne, E.W. Magee, M.J. May and F.S. Porter, Rev. Sci. Instrum. 81 (2010) 10E319

[7] J.L. Schwob, A.W. Wouters, S. Suckewer and M. Finkenthal, Rev. Sci. Instrum. 58 (9) (1987) 1601

[8] R. Prakash, J. Jain, V. Kumar, R. Manchanda, B. Agarwal, M.B. Chowduri, S. Banerjee and P. Vasu, J. Phys. B 43 (2010) 144012

[9] J.E. Manson, Manson model 5 ultrasoft-X ray calibration source,1985; Austin Instruments Inc.

[10] D. Stutman, S. Kovnovich, M. Finkenthal, A. Zwicker and H.W. Moos, Rev. Sci. Instrum. 62 (1991) 2719

[11] C. Breton and J. L. Schwob, C. R. Acad. Sc. 260 (1965) 461

[12] H. P. Summers, *Atomic Data and Analysis Structure User Manual* (2007) http://www.adas.ac.uk/

[13] D. Villegas, R. Guirlet, C. Bourdelle, X. Garbet, G.T. Hoang, R. Sabot, F. Imbeaux and J.L. Ségui, Nucl. Fusion 54 (2014) 073011

[14] C. Biedermann, R. Radtke, J.L. Schwob, P. Mandelbaum, R. Doron, T. Fuchs and G. Fussmann, Physica Scripta T92 (2001) 85

[15] R. Radtke, C. Biedermann, J.L. Schwob, P. Mandelbaum and R. Doron, Phys. Rev. A 64 (2001) 012720